Check for updates

Geophysical Research Letters

RESEARCH LETTER
10.1029/2022GL101773

Key Points:

- Community Earth System Model version 2-large ensemble simulations are used to examine the changes in seasonal cycle of Madden-Julian oscillation (MJO) under global warming
- The model projects changes in both the phase and amplitude of the seasonal cycle of the MJO
- The seasonal delay in phase of the MJO is related to the seasonal delay of total precipitation with contributions from surface latent heat

Supporting Information:

Supporting Information may be found in the online version of this article.

Correspondence to:

H. X. Bui,
hien.bui@monash.edu

Citation:

Bui, H. X., & Hsu, P.-C. (2023). Projected changes in the seasonal cycle of Madden-Julian oscillation precipitation and wind amplitude. *Geophysical Research Letters*, *50*, e2022GL101773. https://doi.org/10.1029/2022GL101773

Received 16 OCT 2022
Accepted 14 JAN 2023

© 2023. The Authors.
This is an open access article under the terms of the Creative Commons Attribution-NonCommercial-NoDerivs License, which permits use and distribution in any medium, provided the original work is properly cited, the use is non-commercial and no modifications or adaptations are made.

Projected Changes in the Seasonal Cycle of Madden-Julian Oscillation Precipitation and Wind Amplitude

Hien X. Bui[1] and Pang-Chi Hsu[2]

[1]School of Earth, Atmosphere and Environment, ARC Centre of Excellence for Climate Extremes, Monash University, Clayton, VIC, Australia, [2]Key Laboratory of Meteorological Disaster of Ministry of Education, Collaborative Innovation Center on Forecast and Evaluation of Meteorological Disasters, Nanjing University of Information Science and Technology, Nanjing, China

Abstract Although recent studies have examined the responses of annual- and seasonal-mean Madden-Julian oscillation (MJO) activity to global warming, little is known about the seasonal cycle changes that determine the timing of the peak MJO influence on local weather and climate. By analyzing the Community Earth System Model version 2 large ensemble at the end of the 21st century, we report changes in both the phase and amplitude of the seasonal cycle of MJO precipitation over the tropical Indian Ocean and southwestern Pacific. While the seasonal delay in phase of the MJO is related to the seasonal delay of total precipitation, with contributions from surface latent heat flux and circulation changes, the amplification in seasonal amplitude is consistent with the increase in MJO amplitude due to mean temperature increases. The shifts in phase of the seasonal cycle of the MJO under global warming may influence the predictability of extreme events.

Plain Language Summary We used the Community Earth System Model version 2 large ensemble simulations to examine the changes in the seasonal cycle of Madden-Julian oscillation (MJO) at the end of the 21st century. Under global warming, models project changes in both the phase and amplitude of seasonal cycle of MJO precipitation over the tropical Indian Ocean and southwestern Pacific. The seasonal delay in peak phases of the MJO precipitation is influenced by the seasonal delay of total precipitation that was modulated by the changes in surface latent heat flux and circulation. We also note that the amplification in seasonal amplitude of the MJO is related to the enhanced MJO amplitude due to mean temperature increases. The novelty of this paper lies in the investigation of seasonal changes of the MJO in response to global warming that are distinct from the annual- and seasonal-mean MJO changes that have been examined in previous studies.

1. Introduction

The Madden-Julian oscillation (MJO; Madden & Julian, 1971, 1972) is a planetary-scale eastward-propagating tropical convective system that has profound impacts on both weather and climate across the globe (Zhang, 2005, 2013). Although a significant peak of MJO occurs during January–March, the MJO shows a seasonal dependence in spatial distribution, amplitude, and propagation characteristics (e.g., Madden & Julian, 1994; Salby & Hendon, 1994; B. Wang & Rui, 1990). The core region of MJO activity is located at low latitudes (e.g., 0°–15°) in the summer hemisphere (Hendon & Liebmann, 1990; Maloney & Kiehl, 2002), which is strongly related to the sea surface temperature (SST) pattern (Zhang & Dong, 2004). During the extended boreal winter (November–April), the MJO is more active with the eastward propagation across the Indo-Pacific warm pool as well as southward propagation toward the South Pacific Convergence Zone (SPCZ; Wheeler & Hendon, 2004). In contrast, during the extended boreal summer (May–October), the MJO shifts toward the Northern Hemisphere (NH) and exhibits a north-northeastward propagation toward the Asian monsoon regions (e.g., DeMott et al., 2013; Jiang et al., 2004; Shukla, 2014; B. Wang & Rui, 1990). Seasonal change in extreme active MJO events has been observed with the increased frequency in March–May and a relatively reduced frequency of occurrences during June–August (Lafleur et al., 2015). The seasonal cycle of the MJO is ultimately driven by solar insolation but could also be modulated by other thermodynamic and dynamic factors, such as land-ocean distribution, land surface properties, and ocean heat fluxes (Lu & Hsu, 2017).

Previous studies have examined changes to the MJO under global warming but have tended to focus on the annual- or seasonal-mean changes in MJO characteristics (e.g., Bui & Maloney, 2019a, 2019b, 2022; Maloney

19448007, 2023, 2, Downloaded from https://agupubs.onlinelibrary.wiley.com/doi/10.1029/2022GL101773 by NHMRC National Cochrane Australia, Wiley Online Library on [29/01/2023]. See the Terms and Conditions (https://onlinelibrary.wiley.com/terms-and-conditions) on Wiley Online Library for rules of use; OA articles are governed by the applicable Creative Commons License

19448007, 2023, 2, Downloaded from https://agupubs.onlinelibrary.wiley.com/doi/10.1029/2022GL101773 by NHMRC National Cochrane Australia, Wiley Online Library on [29/01/2023]. See the Terms and Conditions (https://onlinelibrary.wiley.com/terms-and-conditions) on Wiley Online Library for rules of use; OA articles are governed by the applicable Creative Commons License

et al., 2019). Scant attention has been devoted to the changes in the seasonal cycle of the MJO. In fact, climate models projected a delay in phase (i.e., timing of the amplitude peak) and a reduction in amplitude of the seasonal cycle of global surface temperature under anthropogenic warming scenarios (Dwyer et al., 2012). The change in seasonal cycle of surface temperature is mainly due to the melting of sea ice and the warming of annual mean SST (Biasutti & Sobel, 2009; Dwyer et al., 2012). Such changes in surface temperature can lead to a seasonal delay of tropical precipitation, especially over the monsoonal regions (Biasutti & Sobel, 2009; Song et al., 2018a, 2018b). Dwyer et al. (2014) found that the phase delays in the annual cycle of tropical precipitation appear over both land and ocean areas with a more robust seasonal delay of precipitation maximum over land under global warming. By analyzing the moist static energy (MSE) budget equation, Song et al. (2020) showed that the increased effective atmospheric heat capacity causes a delay in the rainfall season over land, while the land-ocean rainfall contrast during the peak rainfall season favors an early rainfall season over the ocean. The amplitude of the annual tropical rainfall annual cycle is also projected to increase (Chou et al., 2007; Chou & Lan, 2012; Geng et al., 2020; Huang et al., 2013) due to increased lower tropospheric moisture and deceased gross moist stability (Chou et al., 2009). Whether the MJO's seasonal cycle will also change under global warming are still unknown.

By analyzing the National Center for Atmospheric Research (NCAR) Community Earth System Model version 2-large ensemble (CESM2-LE; Rodgers et al., 2021) that has been documented to accurately simulate the MJO (Danabasoglu et al., 2020), we investigate the potential changes in the seasonal cycle of the MJO. The CESM2-LE data set allows us to better characterize the range of internal climate variability, especially with a more realistic treatment of seasonal variability (Haugen et al., 2018). In this paper, we focus on changes to the peak phase and amplitude of the seasonal cycle of the MJO in a future warmer climate and discuss possible factors responsible for these changes. Since the MJO is an important source of predictability for forecasts beyond 2 weeks (Johnson et al., 2014), the shifts in peak phase of the seasonal cycle of the MJO by the end of 21st century may influence the predictability of extreme weather and climate events, especially at the subseasonal-to-seasonal timescale. The results also imply that better monitoring and prediction of the MJO, its teleconnections and influences on extreme events may be required in a future warmer climate.

2. Methods

We use daily mean precipitation and wind from the NCAR CESM2-LE (Rodgers et al., 2021) at a resolution of 1.9° × 2.5° (latitude × longitude). To investigate how the seasonal cycle of MJO changes under global warming, we compare the historical (HIST) climate (1981–2010) using the HIST simulation and the future climate (2071–2100) using Shared Socioeconomic Pathway with fossil-fueled development combined with a 7 W/m^2 forcing scenario (SSP370; O'Neill et al., 2016), where global mean temperature is projected to increase by 4.4°C with a likely range of 3°–5°C by the end of 21st century relative to the HIST climate. Here, we consider a total of 100 ensemble members where the first 50 ensemble members (1–50) are prescribed with biomass burning emission following the Coupled Model Intercomparison Project Phase 6 (CMIP6) protocol (Van Marle et al., 2017) and the second set of 50 members (51–100) follows a smoothed biomass burning. Differences in biomass burning forcing has been shown to affect temperature in the NH extratropics due to changes in cloud cover (see Fasullo et al., 2022).

To understand the changes in the seasonal cycle of the MJO under global warming, all the data (except for those used to calculate the climatological mean) are first bandpass filtered to 20–100 days to retain timescales characteristic of the MJO band (Bui & Maloney, 2018, 2019b). The amplitude of the MJO is defined by analyzing the ensemble-wise standard deviation (i.e., standard deviation across ensemble members) of the band-pass filtered fields (e.g., Bódai et al., 2020; Branstator & Teng, 2010; Herein et al., 2017; Leith, 1978). As described by Rodgers et al. (2021), the ensemble-wise approach can appropriately handle spatially correlated data when considering the confidence intervals (also known as the block bootstrap method) and allows us to better characterize the entire range of climate variability, such as seasonal variability (Haugen et al., 2018). We conducted several sensitivity tests that showed the results do not quantitatively and qualitatively change between the ensemble-wise or time-wise (i.e., standard deviation over time) approaches (see Figures S1 and S2 in Supporting Information S1). In addition, the conclusions of this study are also not sensitive to the biomass burning in model simulations (not shown).

To investigate the changes in phase (defined as timing of the amplitude peak) and amplitude of the seasonal cycle of the MJO, we perform a Fourier transformation analysis on the daily ensemble-wise standard deviation

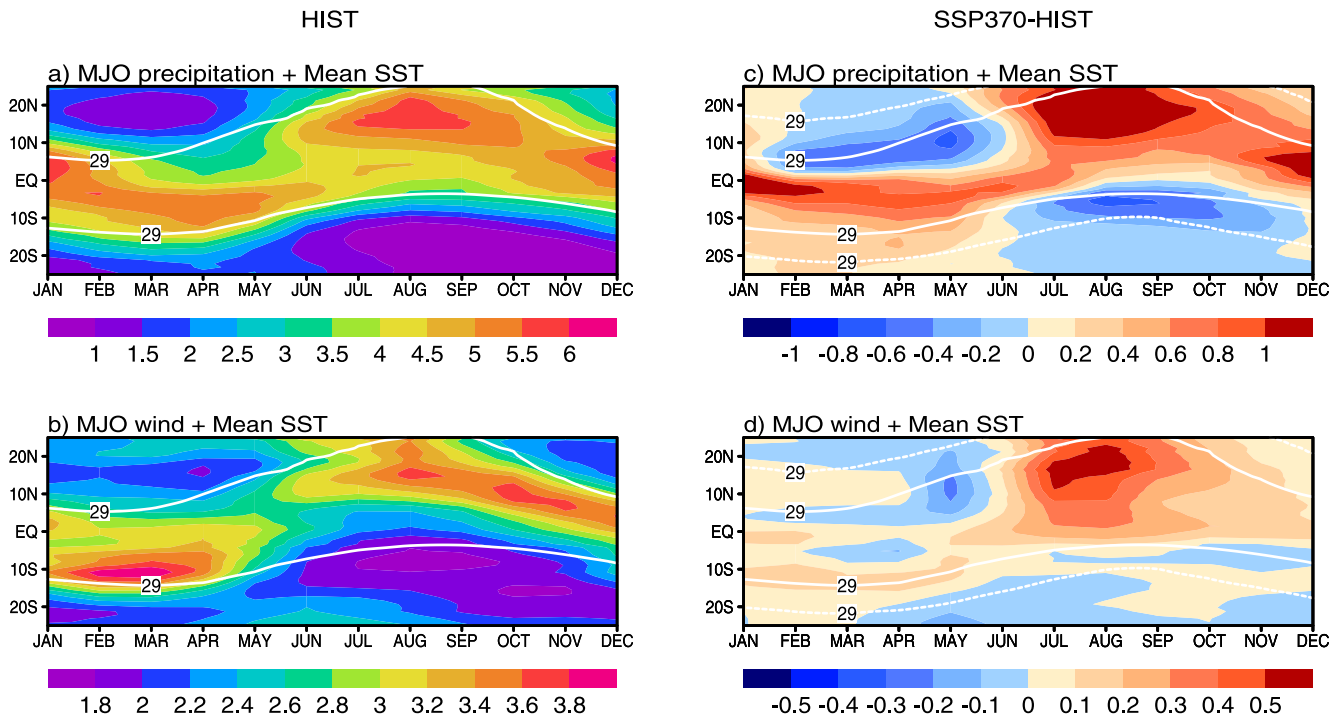

Figure 1. Seasonal evolution of Madden-Julian oscillation (MJO) (a) precipitation (shaded, units are mm/day) and (b) 850 hPa zonal wind (shaded, units are m/s) amplitude averaged over the warm pool (60°E–180°) for the historical (HIST) simulation (1981–2010). (c and d) Similar to (a and b) but for the differences between SSP370 (2071–2100) and HIST simulations (shaded). Contours are mean surface temperature (units are °C; solid is for the HIST simulation while the dotted is for the SSP370 simulation). See Figure S3 in Supporting Information S1 for the climatological mean precipitation and wind, and Figure S9 in Supporting Information S1 for the spatial distribution of MJO filtered precipitation.

precipitation and 850 hPa zonal wind to retain the first two harmonic cycles (e.g., Lu & Hsu, 2017; Zhang & Dong, 2004). The phase of the seasonal cycle is then defined as the location of the first maximum of MJO precipitation and wind amplitude while the amplitude of the seasonal cycle is calculated as the square root of the real and imaginary coefficients of the seasonal cycle. The conclusions do not change when we average the daily data to monthly mean to smooth out day-to-day fluctuations and avoid more than two peaks when defining maximum and minimum peak of seasonal cycle. In this study, we only focus on oceanic regions of the tropics to avoid uncertainty to due topographic effects.

3. Results

Figure 1 shows the latitude-month diagram of the MJO amplitude and mean SST averaged over the warm pool (60°E–180°) where the MJO is most active (Zhang & Dong, 2004). The MJO precipitation is high in boreal winter (February–April). The precipitation peak intensifies and shifts northward by July (Figure 1a). The migration follows the belt of high SST (>29°C) that moves from 10°S in the boreal winter to 15°N in the boreal summer. A similar feature also occurs in the MJO wind amplitude, although the band of strong winds is narrower than that of MJO precipitation (cf., Figures 1a and 1b). During the boreal summer, the MJO reaches its peak at around 20°N and then moves southward to the Southern Hemisphere (SH) beginning the next annual cycle development, resembling the observed distribution (e.g., Zhang & Dong, 2004). For comparison, we also examine the climatological mean fields (Figure S3 in Supporting Information S1) that show the NH precipitation reaches maximum in boreal summer and minimum in boreal winter, and vice versa for the SH. This variation is consistent with the seasonal movement of the tropical convection zone, which has its maximum convection over the summer hemisphere (Chou & Lan, 2012).

Under global warming, the region of warmer SSTs shows a poleward expansion, consistent with a previous study (Dwyer et al., 2012). MJO amplitude is seasonally dependent (Figures 1c and 1d). In general, changes in the seasonal cycle of MJO precipitation follow the "rich-get-richer" (Chou et al., 2009) and "wet-get-wetter"

19448007, 2023, 2, Downloaded from https://agupubs.onlinelibrary.wiley.com/doi/10.1029/2022GL101773 by NHMRC National Cochrane Australia, Wiley Online Library on [29/01/2023]. See the Terms and Conditions (https://onlinelibrary.wiley.com/terms-and-conditions) on Wiley Online Library for rules of use; OA articles are governed by the applicable Creative Commons License

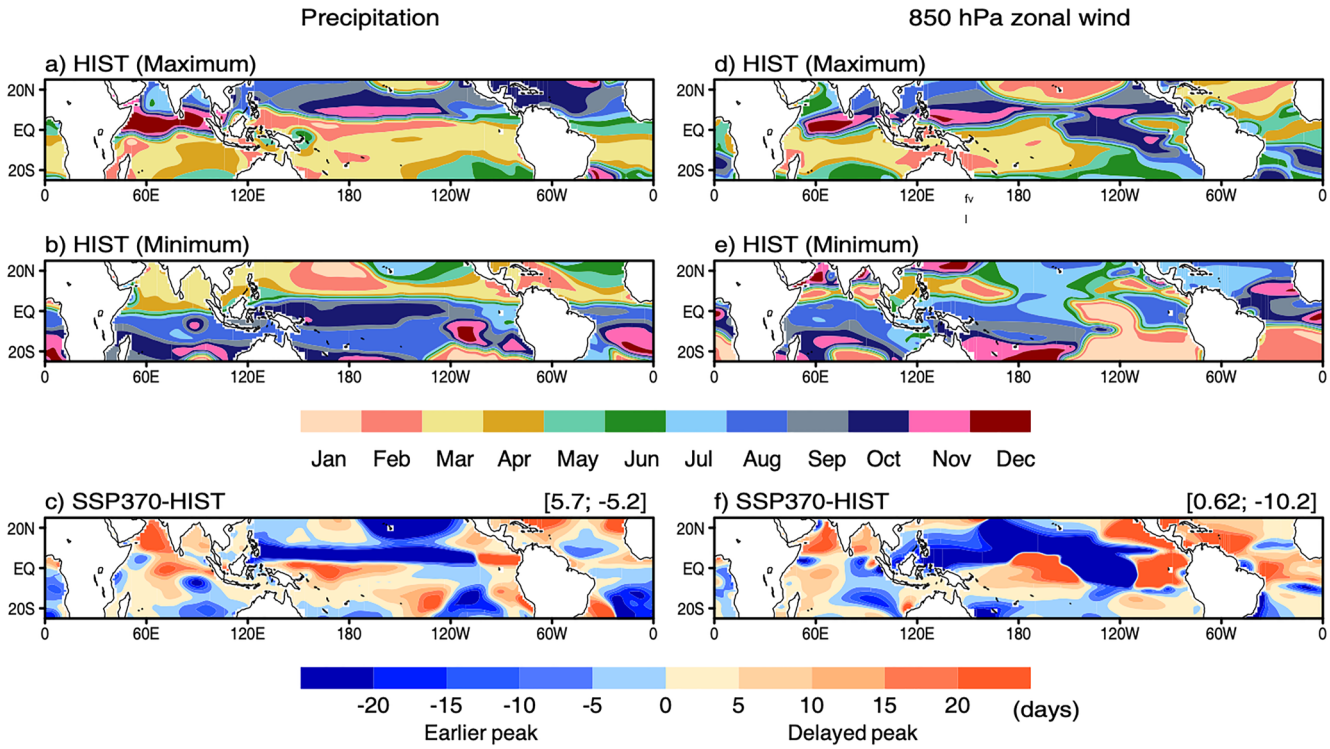

Figure 2. (a and b) Historical (HIST) simulation (1981–2010) of month when the (a) maximum and (b) minimum of the seasonal cycle of Madden-Julian oscillation (MJO) precipitation occur. (c) Differences in the maximum peak (or changes in seasonal phase; units are days) of MJO precipitation between the SSP370 (2081–2100) and HIST simulations. (d–f) Same as (a–c) but for the MJO 850 hPa zonal wind amplitude. Numbers on the top right of (c and f) show the values average over the Indian Ocean (15°S–15°N, 60°–120°E) and western Pacific (15°S–15°N, 120°E–170°W), respectively. Similar plots for the SSP370 simulation are shown in Figure S4 in Supporting Information S1. Differences between the maximum and minimum peak (i.e., a minus b) are shown in Figure S8 in Supporting Information S1.

mechanisms (Xie et al., 2010), marked by enhanced rainfall variability at intraseasonal timescales in a wetter and warmer region and vice versa. Changes in MJO precipitation amplitude exhibit a dipole structure in both hemispheres, such that the amplitude decreases by around 5%–15% during February–May in the NH and during July–October in the SH (Figure 1c). The changes in the seasonal cycle also occur in the MJO wind amplitude, although there is only one enhanced peak during the boreal summer in the NH (Figure 1d). In general, the projected MJO amplitude is enhanced/weakened during the seasons when it is strong/weak in the present-day climate, implying an amplification of the seasonal cycle.

3.1. Phase of the Seasonal Cycle of the MJO

We further examine the seasonal cycle of the MJO by mapping the months with the maximum and the minimum (i.e., the smallest value) MJO amplitude (Figure 2). In the NH, the maximum peak of MJO precipitation generally occurs in July–September over the Northern Indian Ocean regions, and in November–December over the equatorial Indian Ocean. Notably, there is a peak during February–April over the equatorial regions in Pacific Ocean. In the SH, the patterns are more uniform and generally follow latitude bands with the maximum peaks occurring during March and April (Figure 2a). Over most regions, the months with maximum and minimum MJO precipitation are 6 ± 1 month apart (cf., Figures 2a and 2b; see also Figure S8 in Supporting Information S1). However, this is not always the case, especially near the equatorial Pacific, where the seasonal cycle of MJO precipitation exhibits a secondary peak, which likely corresponds to the oscillation of the Intertropical Convergence Zone. Interestingly, there is a sharp jump in the timing of maximum peak near the central north Pacific (i.e., northeast of the Hawaiian Islands), which potentially reflects the influence of other processes and could be subject to further investigations.

Under global warming, over the Indian Ocean and SPCZ regions, the seasonal peak of MJO precipitation occurs about 1–2 weeks later relative to the current climate (regions with a positive anomaly in Figure 2c). The delay in

19448007, 2023, 2, Downloaded from https://agupubs.onlinelibrary.wiley.com/doi/10.1029/2022GL101773 by NHMRC National Cochrane Australia, Wiley Online Library on [29/01/2023]. See the Terms and Conditions (https://onlinelibrary.wiley.com/terms-and-conditions) on Wiley Online Library for rules of use; OA articles are governed by the applicable Creative Commons License

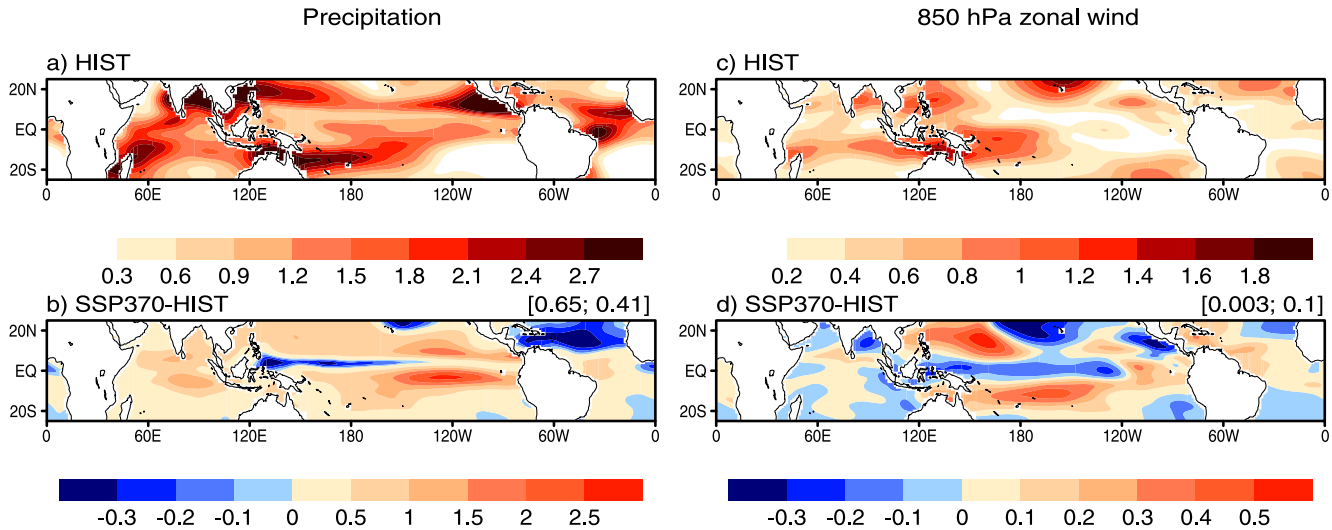

Figure 3. (a and c) Historical (HIST) simulation of the seasonal amplitude of Madden-Julian oscillation (MJO) precipitation (units are mm/day) and 850 hPa zonal wind (units are m/s), respectively. (c and d) Differences in seasonal amplitude of MJO precipitation and wind in the SSP370 relative to HIST simulations. Numbers on the top right of (b and d) show the values average over the Indian Ocean (15°S–15°N, 60°–120°E) and western Pacific (15°S–15°N, 120°E–170°W), respectively.

seasonal phase of the MJO also occurs over the northeastern Pacific. However, there are also several regions of phase advance (negative anomalies in Figure 2c), such that models predict the seasonal peak of MJO precipitation to occur about 3 weeks earlier over the northern Pacific in response to global warming.

The distribution of maximum and minimum peaks of the 850 hPa zonal wind amplitude associated with the MJO (Figures 2d and 2e) are broadly similar to that of MJO precipitation, although the maximum peak of MJO wind seems to occur slightly before the peak MJO precipitation (cf., Figures 2a and 2d). The patterns of MJO winds are less zonally uniform than that of MJO precipitation, especially over the eastern Pacific (cf., Figures 2a–2d, 2e). Under global warming, the phase of the seasonal cycle of MJO wind is generally in phase with that of MJO precipitation (cf., Figures 2f and 2c), although when averaging over the entire tropics, the maximum peaks of MJO precipitation are more delayed than that of MJO wind in the future. The seasonal phase of both MJO precipitation and wind tend to be delayed over the Indian Ocean but advanced over the western Pacific (e.g., see the number on the top right of Figures 2c and 2f).

3.2. Amplitude of the Seasonal Cycle of the MJO

In addition to the changes in MJO peak phase timing, we also examine the seasonal amplitude of the MJO (see Section 2 and Figure 3). MJO precipitation shows a large seasonal amplitude over the Indo-Pacific and northern Australia regions (Figure 3a), resembling the climatological mean pattern (not shown). There is also a peak amplitude over the northeastern Pacific which is an intraseasonal mode of variability that is isolated from the Eastern Hemisphere, although variability in this region tends to phase-lock with the MJO (Jiang et al., 2012). A smaller seasonal amplitude near the equator might be due to a smaller annual variability in solar insolation. The seasonal amplitude of the MJO wind pattern is broadly similar to that of the MJO precipitation but tends to be located closer to the equator, especially in the eastern hemisphere (Figure 3c).

Under global warming, MJO precipitation shows an amplification in the seasonal amplitude, such that there is a greater difference between the annual maximum and minimum over most of the tropics relative to the HIST simulation (Figure 3b). Greater amplitudes are found not only in the Indian Ocean but also in the central and eastern Pacific where the seasonal amplitude is large in the current climate. The enhanced seasonal amplitude of MJO over the central and eastern Pacific may be related to the extension of the MJO (Bui & Maloney, 2018) and/or warmer surface temperatures (e.g., an El Niño-like warming pattern). Interestingly, there is a reduction in seasonal amplitude over the narrow band of the equatorial region east of Borneo Island and the northern Atlantic, which is different from the change in the MJO amplitude itself (Bui & Maloney, 2018, 2019a, 2019b; Maloney et al., 2019), thus deserving further examination.

19448007, 2023, 2, Downloaded from https://agupubs.onlinelibrary.wiley.com/doi/10.1029/2022GL101773 by NHMRC National Cochrane Australia, Wiley Online Library on [29/01/2023]. See the Terms and Conditions (https://onlinelibrary.wiley.com/terms-and-conditions) on Wiley Online Library for rules of use; OA articles are governed by the applicable Creative Commons License

19448007, 2023, 2, Downloaded from https://agupubs.onlinelibrary.wiley.com/doi/10.1029/2022GL101773 by NHMRC National Cochrane Australia, Wiley Online Library on [29/01/2023]. See the Terms and Conditions (https://onlinelibrary.wiley.com/terms-and-conditions) on Wiley Online Library for rules of use; OA articles are governed by the applicable Creative Commons License

The enhancement of the seasonal cycle amplitude of MJO wind tends to concentrate over the northwestern and southwestern Pacific regions only. The seasonal cycle amplitude of MJO wind changes by less than that of MJO precipitation, consistent with previous studies that showed a reduction of MJO wind amplitude due to the mean temperature increase (Bui & Maloney, 2018, 2019a, 2019b; Maloney et al., 2019). Notably, the changes in phase and amplitude of the seasonal cycle of the MJO are not in the same sign everywhere (cf., Figures 2c, 2f and 3b, 3d), implying different mechanisms for the change, which will be discussed below.

3.3. Possible Mechanisms

It has been established that latent heat flux has a positive covariance with intraseasonal precipitation in the current climate (Araligidad & Maloney, 2008; Bui et al., 2020) and that the seasonal cycle of MJO variance is strongly connected to that of the mean state in the current climate (Zhang & Dong, 2004). Two major theories for MJO dynamics: moisture mode theory (Sobel & Maloney, 2012, 2013) and wind-induced surface heat exchange (WISHE) theory (Raymond & Fuchs, 2018) both place latent heat flux as an important factor for maintaining the MJO. The moisture mode theory relies on surface fluxes working in tandem with radiative feedbacks and horizontal moisture advection to enhance MSE ahead of the MJO, while for WISHE, only wind-driven fluxes are important. The change in seasonality of the surface heat flux has been found to control the change in phase and amplitude of surface temperature over the tropics in an energy balance model (Dwyer et al., 2012). The phase delay in surface temperature due to the increased heat capacity over the ocean then favors a phase delay in tropical precipitation under the atmospheric energy constraint (Song et al., 2020). Moreover, the ocean also diverts more of the anomalous incoming energy into latent heat rather than increasing surface temperature (Seth et al., 2013; Sutton et al., 2007).

To build on these previous works, we examine the relationship between the changes in phase of seasonal cycle of the MJO (y-axis) and the background mean state (x-axis) averaged over the Indian ocean and western Pacific domains (Figures 4a–4d) where the MJO signals are strongest (e.g., Bui et al., 2020, among many others). Results shown are not sensitive to the exact bounds used for these regional averages. In Figure 4, each dot represents an average of 10 sub-groups in the CESM2-LE (Rodgers et al., 2021) to reduce the uncertainty from different members with different initial conditions. Although the impacts of model initial conditions on the MJO characteristics would be expected, quantifying these effects is a topic of future work. Based on current analysis, there are several possible factors influencing the changes to the seasonal cycle of the MJO.

- *Mean Precipitation*: The correlation between changes in seasonal phase of MJO precipitation and total precipitation are 0.82 over the Indian Ocean, suggesting that the delayed seasonal cycle of MJO precipitation is associated with a delayed seasonal cycle of mean precipitation (Figure 4a). Notably, over the Pacific, MJO precipitation is delayed but the total mean precipitation is earlier, suggesting other factors contribute to the change and deserve further analysis. This result is in agreement with previous studies that focus on the dynamic of the climatological mean state changes (Biasutti & Sobel, 2009; Song et al., 2018a, 2018b). The result also confirms the strong connection between the seasonal cycle of the MJO and the seasonal cycle of the mean state as shown in the current climate (e.g., Zhang & Dong, 2004).
- *Surface Latent Heat Flux*: The regression coefficient between latent heat flux and MJO precipitation indicates that changes in the seasonal phase of MJO precipitation are greater than the changes in the seasonal phase of latent heat flux in both ocean regions (with a correlation of 0.66 over the western Pacific and a correlation of 0.47 over the Indian Ocean; Figure 4b). Notably, model members with a larger seasonal delay in mean latent heat flux exhibit a larger seasonal delay in MJO precipitation. We also note that the connection is clear for the MJO's wind over the Indian and Pacific Oceans (not shown).
- *Circulation*: As shown in Figure 4c, all model members occur around the line of slope 1, indicating a strong relationship between the seasonal cycle changes of MJO precipitation and mean circulation over the target domains (with the correlation coefficient of 0.79 over the Indian Ocean and 0.63 over the western Pacific).
- *Temperature*: It is surprising that the changes in peak phase of seasonal cycle of the MJO are not well correlated with that of mean surface temperature (e.g., low or even negative correlation coefficient over the Indian Ocean). This result is different from previous reports about the strong relationship between surface temperature and the seasonal cycle of total precipitation in the current climate (Biasutti & Sobel, 2009). As shown in Figure 4d, the seasonal cycle of SSTs tends to be delayed more over the Indian Ocean than over the western Pacific in a warmer climate. A more delayed seasonal cycle of SSTs is associated with a more delayed seasonal cycle of MJO precipitation when comparing across model members and regions.

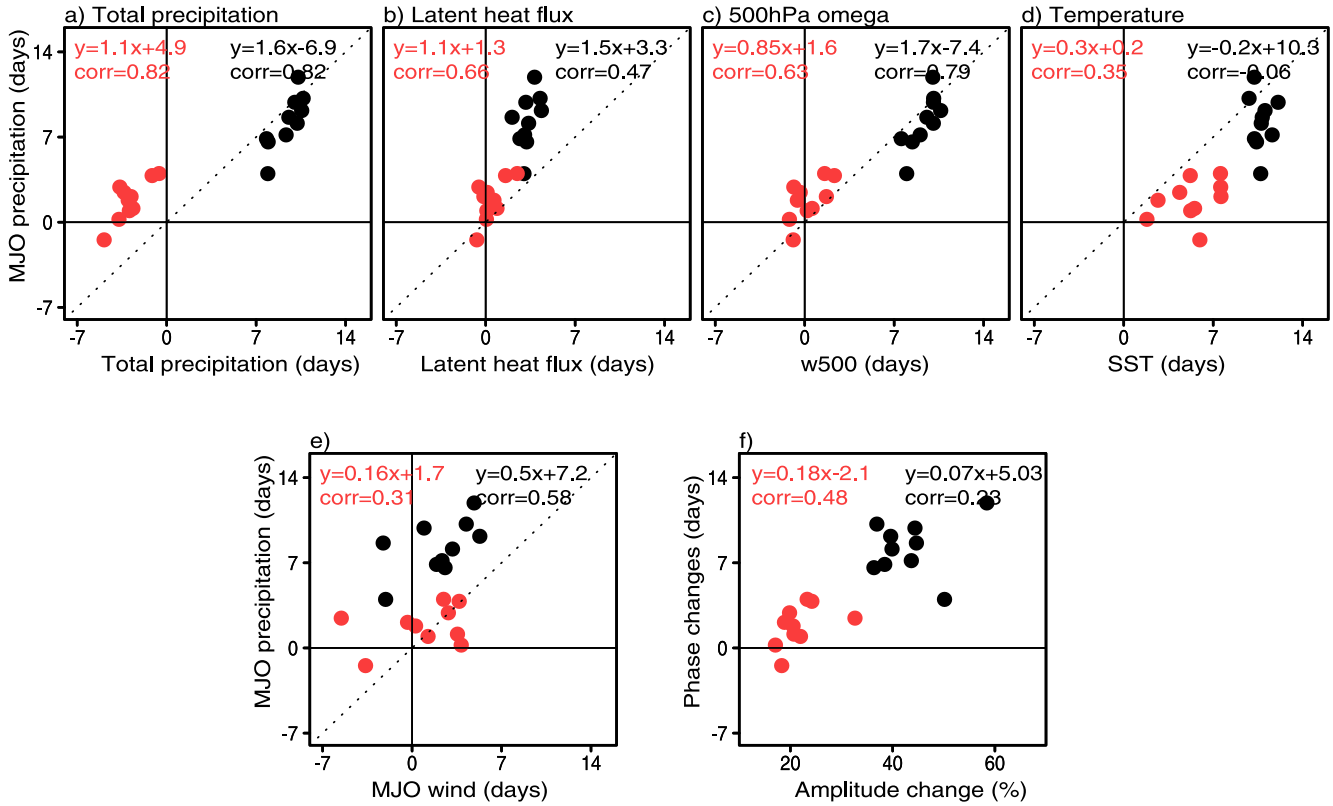

Figure 4. Differences in the phase (units are days) of seasonal cycle of Madden-Julian oscillation (MJO) precipitation (*y*-axis) versus differences in phase of several climatological variables (*x*-axis): (a) total precipitation, (b) surface latent heat flux, (c) 500 hPa omega, and (d) sea surface temperature. (e) Differences in seasonal phase of MJO precipitation and MJO wind (units are days). (f) Differences between seasonal phase change (positive indicates a delayed peak while negative indicates an earlier peak; units are days) and seasonal amplitude change (units are %) of MJO precipitation. Dots represent an averaged of 10 sub-groups in the Community Earth System Model version 2-large ensemble. Red dots represent Pacific Ocean (15°S-Eq., 130°–150°E) and black for Indian Ocean (15°S–10°N, 60°–90°E) averaged. The dotted line shows a 1:1 relationship.

We also examine the differences between MJO precipitation and wind. The result shows that the seasonal phase of MJO precipitation tends to delay more than that of MJO wind and the delay is more evident over the Indian Ocean than western Pacific (Figure 4e). The changes in seasonal amplitude of MJO precipitation are larger over the Indian Ocean than western Pacific in the future climate, which may be due to a greater increase of vertical moisture gradient in a warmer climate (see Bui & Maloney, 2019a). The changes in the seasonal cycle amplitude of the MJO does not seem to play a major role in explaining the inter-ensemble spread of the changing seasonal phase of the MJO (Figure 4f).

Some features seen in Figure 4 need additional scrutiny. Over the tropical oceans, higher wind speeds are generally associated with larger surface heat fluxes and thus enhanced precipitation and convection (Bui et al., 2020). Previous studies found the significant contribution of latent heat flux to the column-integrated intraseasonal MSE budget (Maloney, 2009). However, it is unclear whether the latent heat flux is still dominated by a wind component in a warmer climate, or if it will be controlled by SSTs as the tropical circulation weakens. There is also a question about how the correlation between SSTs and the MJO seasonal cycle changes under global warming as they are highly correlated in the current climate (Figure 4d). We have further examined the changes in seasonal phase and amplitude of several mean state variables (Figures S5–S7 in Supporting Information S1). The similar pattern between total precipitation and low-level specific humidity confirms the previous argument that changes in the seasonal cycle of precipitation is associated with changes in lower tropospheric humidity (Chou et al., 2009).

There are a few caveats to the results shown here. The MJO has its own phase evolution in its life cycle and there are certainly phase dependences. Additionally, we did not analyze the seasonal cycle based on individual MJO events, but instead use the standard deviation of filtered fields to find the overall features related to the MJO

19448007, 2023, 2, Downloaded from https://agupubs.onlinelibrary.wiley.com/doi/10.1029/2022GL101773 by NHMRC National Cochrane Australia, Wiley Online Library on [29/01/2023]. See the Terms and Conditions (https://onlinelibrary.wiley.com/terms-and-conditions) on Wiley Online Library for rules of use; OA articles are governed by the applicable Creative Commons License

19448007, 2023, 2, Downloaded from https://agupubs.onlinelibrary.wiley.com/doi/10.1029/2022GL101773 by NHMRC National Cochrane Australia, Wiley Online Library on [29/01/2023]. See the Terms and Conditions (https://onlinelibrary.wiley.com/terms-and-conditions) on Wiley Online Library for rules of use; OA articles are governed by the applicable Creative Commons License

seasonal cycle. An alternative method would be to track the individual MJO events, however we favor our current method for the ease of reproducibility and independence of MJO case identification methods. The geographic distribution of maximum and minimum fields as well as the amplitude of the seasonal cycle (Figures 2 and 3) gives us confidence that the current approach does not alter our conclusions.

4. Concluding Remarks

In this study, we use 100 ensemble members from the CESM2-LE that has been documented to have a realistic MJO simulation, to study how the seasonal cycle of MJO precipitation and wind amplitude is projected to change by the end of the 21st century relative to HIST climate under the SSP370 scenario. Compared to previous studies that have examined the changes in annual- or seasonal-mean MJO activity, our current study is the first to assess the changes to MJO seasonality under global warming and discuss possible factors accounting for these changes in a large ensemble data set. Under SSP370, the model projects a delay in the peak phase and an amplification in the amplitude of the seasonal cycle of MJO precipitation over most areas with an active MJO in the present climate. The maximum peak of MJO precipitation tends to occur about 1–2 weeks later in the year and shows a greater difference between annual maximum and minimum over the tropical eastern Indian Ocean and southwestern Pacific (Figures 2 and 3). Our diagnostic results suggest that the seasonal delay in phase of the MJO is influenced by a seasonal delay in total precipitation with contributions from surface latent heat flux and circulation changes, while the amplification in seasonal amplitude is consistent with the increase of MJO amplitude due to a mean temperature increase (Figure 4).

The results presented in this paper agreed well with earlier papers about the variations in MJO seasonality observed in the recent decades (Lu & Hsu, 2017; Zhang & Dong, 2004) with an extension to a future warmer climate. Since the MJO is the dominant mode of intraseasonal variability in the global atmosphere that contributes to extratropical teleconnections in summer, our results imply a potential delay in seasonality impacts of the MJO on North American temperature (Baggett et al., 2018; Jenney et al., 2019; L. Wang et al., 2013) as well as interactions between the MJO and other phenomena (Adames et al., 2016) in a future warmer climate. We speculate that the changes in the seasonal peak of the MJO amplitude shown here, and its associated circulation, might have influences on atmospheric Rossby waves and thus extratropical teleconnections and forecasts, especially at the subseasonal-to-seasonal timescale. Future work will verify the current results using a broader set of climate models like CMIP5/6, which may show a greater range of potential MJO changes under global warming. We are also interested in examining the underlying reason and consequences of the delayed peak of the seasonal cycle of the MJO amplitude.

Data Availability Statement

The CESM2-LE outputs can be downloaded at https://www.cesm.ucar.edu/projects/community-projects/LENS2/data-sets.html.

Acknowledgments
We thank two anonymous reviewers for detailed comments that significantly improved the manuscript. We also thank Peter van Rensch and Kimberley Reid (Monash University) for reading and comment on the manuscript. The authors acknowledge June-Yi Lee and Ji-Eun Kim (Pusan National University) for discussion that motivate the current study, and Yi-Xian Li (National Central University) for suggestion about processing codes. We also acknowledge NCAR and IBS Center for Climate Physics for providing the CESM2-LE data. This work was supported by Australian Research Council under Grant CE170100023. PCH was supported by National Natural Science Foundation of China under Grant 4225502. Open access publishing facilitated by Monash University, as part of the Wiley - Monash University agreement via the Council of Australian University Librarians.

References

Adames, Á. F., Wallace, J. M., & Monteiro, J. M. (2016). Seasonality of the structure and propagation characteristics of the MJO. *Journal of the Atmospheric Sciences*, *73*(9), 3511–3526. https://doi.org/10.1175/jas-d-15-0232.1

Araligidad, N. M., & Maloney, E. D. (2008). Wind-driven latent heat flux and the intraseasonal oscillation. *Geophysical Research Letters*, *35*(4), L04815. https://doi.org/10.1029/2007GL032746

Baggett, C. F., Nardi, K. M., Childs, S. J., Zito, S. N., Barnes, E. A., & Maloney, E. D. (2018). Skillful subseasonal forecasts of weekly Tornado and Hail activity using the Madden-Julian oscillation. *Journal of Geophysical Research: Atmospheres*, *123*(22), 12661–12675. https://doi.org/10.1029/2018JD029059

Biasutti, M., & Sobel, A. H. (2009). Delayed Sahel rainfall and global seasonal cycle in a warmer climate. *Geophysical Research Letters*, *36*(23), L23707. https://doi.org/10.1029/2009GL041303

Bódai, T., Drótos, G., Herein, M., Lunkeit, F., & Lucarini, V. (2020). The forced response of the El Niño–Southern Oscillation–Indian monsoon teleconnection in ensembles of Earth system models. *Journal of Climate*, *33*(6), 2163–2182. https://doi.org/10.1175/jcli-d-19-0341.1

Branstator, G., & Teng, H. (2010). Two limits of initial-value decadal predictability in a CGCM. *Journal of Climate*, *23*(23), 6292–6311. https://doi.org/10.1175/2010jcli3678.1

Bui, H. X., & Maloney, E. D. (2018). Changes in Madden-Julian oscillation precipitation and wind variance under global warming. *Geophysical Research Letters*, *45*(14), 7148–7155. https://doi.org/10.1029/2018GL078504

Bui, H. X., & Maloney, E. D. (2019b). Mechanisms for global warming impacts on Madden-Julian oscillation precipitation amplitude. *Journal of Climate*, *2*(20), 6961–6975. https://doi.org/10.1175/jcli-d-19-0051.1

Bui, H. X., & Maloney, E. D. (2019a). Transient response of MJO precipitation and circulation to greenhouse gas forcing. *Geophysical Research Letters*, *46*(22), 13546–13555. https://doi.org/10.1029/2019GL085328

Bui, H. X., & Maloney, E. D. (2022). Changes to tropical eastern north Pacific intraseasonal variability under global warming–Implications for tropical cyclogenesis. *Atmósfera*, *35*(4), 611–631. https://doi.org/10.20937/ATM.53021

Bui, H. X., Maloney, E. D., Riley Dellaripa, E. M., & Singh, B. (2020). Wind speed, surface flux, and intraseasonal convection coupling from CYGNSS data. *Geophysical Research Letters*, *47*(21), e2020GL090376. https://doi.org/10.1029/2020GL090376

Chou, C., & Lan, C.-W. (2012). Changes in the annual range of precipitation under global warming. *Journal of Climate*, *25*(1), 222–235. https://doi.org/10.1175/JCLI-D-11-00097.1

Chou, C., Neelin, J., Chen, C., & Tu, J. (2009). Evaluating the "rich-get-richer" mechanism in tropical precipitation change under global warming. *Journal of Climate*, *22*(8), 1982–2005. https://doi.org/10.1175/2008JCLI2471.1

Chou, C., Tu, J.-Y., & Tan, P.-H. (2007). Asymmetry of tropical precipitation change under global warming. *Geophysical Research Letters*, *34*(17), L17708. https://doi.org/10.1029/2007GL030327

Danabasoglu, G., Lamarque, J.-F., Bacmeister, J., Bailey, D. A., DuVivier, A. K., Edwards, J., et al. (2020). The community Earth system model version 2 (CESM2). *Journal of Advances in Modeling Earth Systems*, *12*, e2019MS001916. https://doi.org/10.1029/2019MS001916

DeMott, C. A., Stan, C., & Randall, D. A. (2013). Northward propagation mechanisms of the boreal summer intraseasonal oscillation in the ERA-Interim and SP-CCSM. *Journal of Climate*, *26*(6), 1973–1992. https://doi.org/10.1175/JCLI-D-12-00191.1

Dwyer, J. G., Biasutti, M., & Sobel, A. H. (2012). Projected changes in the seasonal cycle of surface temperature. *Journal of Climate*, *25*(18), 6359–6374. https://doi.org/10.1175/JCLI-D-11-00741.1

Dwyer, J. G., Biasutti, M., & Sobel, A. H. (2014). The effects of greenhouse gas-induced changes in SST on the annual cycle of zonal mean tropical precipitation. *Journal of Climate*, *27*(12), 4545–4565. https://doi.org/10.1175/jcli-d-13-00216.1

Fasullo, J. T., Lamarque, J.-F., Hannay, C., Rosenbloom, N., Tilmes, S., DeRepentigny, P., et al. (2022). Spurious late historical-era warming in CESM2 driven by prescribed biomass burning emissions. *Geophysical Research Letters*, *49*(2), e2021GL097420. https://doi.org/10.1029/2021GL097420

Geng, Y., Xie, S., Zheng, X., & Wang, C. (2020). Seasonal dependency of tropical precipitation change under global warming. *Journal of Climate*, *33*(18), 7897–7908. https://doi.org/10.1175/JCLI-D-20-0032.1

Haugen, M. A., Stein, M. L., Moyer, E. J., & Sriver, R. L. (2018). Estimating changes in temperature distributions in a large ensemble of climate simulations using quantile regression. *Journal of Climate*, *31*(20), 8573–8588. https://doi.org/10.1175/jcli-d-17-0782.1

Hendon, H. H., & Liebmann, B. (1990). The intraseasonal (30–50 day) oscillation of the Australian summer monsoon. *Journal of the Atmospheric Sciences*, *47*(24), 2909–2923. https://doi.org/10.1175/1520-0469(1990)047<2909:tidoot>2.0.co;2

Herein, M., Drótos, G., Haszpra, T., Márfy, J., & Tél, T. (2017). The theory of parallel climate realizations as a new framework for teleconnection analysis. *Scientific Reports*, *7*(1), 44529. https://doi.org/10.1038/srep44529

Huang, P., Xie, S.-P., Hu, K., Huang, G., & Huang, R. (2013). Patterns of the seasonal response of tropical rainfall to global warming. *Nature Geoscience*, *6*(5), 357–361. https://doi.org/10.1038/ngeo1792

Jenney, A. M., Nardi, K. M., Barnes, E. A., & Randall, D. A. (2019). The seasonality and regionality of MJO impacts on North American temperature. *Geophysical Research Letters*, *46*(15), 9193–9202. https://doi.org/10.1029/2019GL083950

Jiang, X., Li, T., & Wang, B. (2004). Structures and mechanisms of the northward propagating boreal summer intraseasonal oscillation. *Journal of Climate*, *17*(5), 1022–1039. https://doi.org/10.1175/1520-0442(2004)017,1022:SAMOTN.2.0.CO.2

Jiang, X., Zhao, M., & Waliser, D. E. (2012). Modulation of tropical cyclones over the eastern Pacific by the intra-seasonal variability simulated in an AGCM. *Journal of Climate*, *25*(19), 6524–6538. https://doi.org/10.1175/JCLI-D-11-00531.1

Johnson, N. C., Collins, D. C., Feldstein, S. B., L'Heureux, M. L., & Riddle, E. E. (2014). Skillful wintertime North American temperature forecasts out to 4 weeks based on the state of ENSO and the MJO. *Weather and Forecasting*, *29*(1), 23–38. https://doi.org/10.1175/waf-d-13-00102.1

Lafleur, D. M., Barrett, B. S., & Henderson, G. R. (2015). Some climatological aspects of the Madden–Julian oscillation (MJO). *Journal of Climate*, *28*(15), 6039–6053. https://doi.org/10.1175/jcli-d-14-00744.1

Leith, C. (1978). Predictability of climate. *Nature*, *276*(5686), 352–355. https://doi.org/10.1038/276352a0

Lu, W., & Hsu, P. C. (2017). Factors controlling the seasonality of the Madden-Julian oscillation. *Dynamics of Atmospheres and Oceans*, *78*, 106–120. https://doi.org/10.1016/j.dynatmoce.2017.04.002

Madden, R. A., & Julian, P. R. (1971). Detection of a 40–50 day oscillation in the zonal wind in the tropical Pacific. *Journal of the Atmospheric Sciences*, *28*(5), 702–708. https://doi.org/10.1175/1520-0469(1971)028<0702:DOADOI>2.0.CO;2

Madden, R. A., & Julian, P. R. (1972). Description of global-scale circulation cells in the tropics with a 40–50 day period. *Journal of the Atmospheric Sciences*, *29*(6), 1109–1123. https://doi.org/10.1175/1520-0469(1972)029<1109:DOGSCC>2.0.CO;2

Madden, R. A., & Julian, P. R. (1994). Observations of the 40–50-day tropical oscillation—A review. *Monthly Weather Review*, *122*(5), 814–837. https://doi.org/10.1175/1520-0493(1994)122,0814:OOTDTO.2.0.CO;2

Maloney, E. D. (2009). The moist static energy budget of a composite tropical intraseasonal oscillation in a climate model. *Journal of Climate*, *22*(3), 711–729. https://doi.org/10.1175/2008JCLI2542.1

Maloney, E. D., Adames, Á. F., & Bui, H. X. (2019). Madden-Julian oscillation changes under anthropogenic warming. *Nature Climate Change*, *9*(1), 26–33. https://doi.org/10.1038/s41558-018-0331-6

Maloney, E. D., & Kiehl, J. T. (2002). MJO-related SST variations over the tropical eastern Pacific during northern hemisphere summer. *Journal of Climate*, *15*(6), 675–689. https://doi.org/10.1175/1520-0442(2002)015<0675:mrsvot>2.0.co;2

O'Neill, B. C., Tebaldi, C., van Vuuren, D. P., Eyring, V., Friedlingstein, P., Hurtt, G., et al. (2016). The scenario model intercomparison project (ScenarioMIP) for CMIP6. *Geoscientific Model Development*, *9*(9), 3461–3482. https://doi.org/10.5194/gmd-9-3461-2016

Raymond, D. J., & Fuchs, Ž. (2018). The Madden-Julian oscillation and the Indo-Pacific warm pool. *Journal of Advances in Modeling Earth Systems*, *10*(4), 951–960. https://doi.org/10.1002/2017MS001258

Rodgers, K. B., Lee, S. S., Rosenbloom, N., Timmermann, A., Danabasoglu, G., Deser, C., et al. (2021). Ubiquity of human-induced changes in climate variability. *Earth System Dynamics*, *12*(4), 1393–1411. https://doi.org/10.5194/esd-12-1393-2021

Salby, M. L., & Hendon, H. H. (1994). Intraseasonal behavior of clouds, temperature, and motion in the Tropics. *Journal of the Atmospheric Sciences*, *51*(15), 2207–2224. https://doi.org/10.1175/1520-0469(1994)051<2207:ibocta>2.0.co;2

Seth, A., Rauscher, S. A., Biasutti, M., Giannini, A., Camargo, S. J., & Rojas, M. (2013). CMIP5 projected changes in the annual cycle of precipitation in monsoon regions. *Journal of Climate*, *26*(19), 7328–7351. https://doi.org/10.1175/jcli-d-12-00726.1

Shukla, R. P. (2014). The dominant intraseasonal mode of intra-seasonal South Asian summer monsoon. *Journal of Geophysical Research: Atmospheres*, *119*(2), 635–651. https://doi.org/10.1002/2013JD020335

Sobel, A., & Maloney, E. D. (2012). An idealized semi-empirical framework for modeling the Madden-Julian oscillation. *Journal of the Atmospheric Sciences*, *69*(5), 1691–1705. https://doi.org/10.1175/JAS-D-11-0118.1

Sobel, A., & Maloney, E. D. (2013). Moisture modes and the eastward propagation of the MJO. *Journal of the Atmospheric Sciences*, *70*(1), 187–192. https://doi.org/10.1175/JAS-D-12-0189.1

19448007, 2023, 2, Downloaded from https://agupubs.onlinelibrary.wiley.com/doi/10.1029/2022GL101773 by NHMRC National Cochrane Australia, Wiley Online Library on [29/01/2023]. See the Terms and Conditions (https://onlinelibrary.wiley.com/terms-and-conditions) on Wiley Online Library for rules of use; OA articles are governed by the applicable Creative Commons License

Song, F., Leung, L. R., Lu, J., & Dong, L. (2018a). Future changes in seasonality of the North Pacific and North Atlantic subtropical highs. *Geophysical Research Letters*, *45*(21), 11959–11968. https://doi.org/10.1029/2018GL079940

Song, F., Leung, L. R., Lu, J., & Dong, L. (2018b). Seasonally dependent responses of subtropical highs and tropical rainfall to anthropogenic warming. *Nature Climate Change*, *8*(9), 787–792. https://doi.org/10.1038/s41558-018-0244-4

Song, F., Lu, J., Leung, L. R., & Liu, F. (2020). Contrasting phase changes of precipitation annual cycle between land and ocean under global warming. *Geophysical Research Letters*, *47*(20), e2020GL090327. https://doi.org/10.1029/2020GL090327

Sutton, R. T., Dong, B., & Gregory, J. M. (2007). Land/sea warming ratio in response to climate change: IPCC AR4 model results and comparison with observations. *Geophysical Research Letters*, *34*(2), L02701. https://doi.org/10.1029/2006GL028164

Van Marle, M. J., Kloster, S., Magi, B. I., Marlon, J. R., Daniau, A. L., Field, R. D., et al. (2017). Historic global biomass burning emissions for CMIP6 (BB4CMIP) based on merging satellite observations with proxies and fire models (1750–2015). *Geoscientific Model Development*, *10*(9), 3329–3357. https://doi.org/10.5194/gmd-10-3329-2017

Wang, B., & Rui, H. (1990). Synoptic climatology of transient tropical intraseasonal convection anomalies: 1975–1985. *Meteorology and Atmospheric Physics*, *44*(1–4), 43–61. https://doi.org/10.1007/BF01026810

Wang, L., Li, T., Zhou, T., & Rong, X. (2013). Origin of the intraseasonal variability over the North Pacific in boreal summer. *Journal of Climate*, *26*(4), 1211–1229. https://doi.org/10.1175/jcli-d-11-00704.1

Wheeler, M. C., & Hendon, H. H. (2004). An all-season real-time multivariate MJO index: Development of an index for monitoring and prediction. *Monthly Weather Review*, *132*(8), 1917–1932. https://doi.org/10.1175/1520-0493(2004)132,1917:AARMMI.2.0.CO;2

Xie, S., Deser, C., Vecchi, G. A., Ma, J., Teng, H., & Wittenberg, A. T. (2010). Global warming pattern formation: Sea surface temperature and rainfall. *Journal of Climate*, *23*(4), 966–986. https://doi.org/10.1175/2009jcli3329.1

Zhang, C. (2005). Madden-Julian oscillation. *Reviews of Geophysics*, *43*(2), RG2003. https://doi.org/10.1029/2004RG000158

Zhang, C. (2013). Madden–Julian oscillation: Bridging weather and climate. *Bulletin of the American Meteorological Society*, *94*(12), 1849–1870. https://doi.org/10.1175/BAMS-D-12-00026.1

Zhang, C., & Dong, M. (2004). Seasonality in the Madden–Julian oscillation. *Journal of Climate*, *17*(16), 3169–3180. https://doi.org/10.1175/1520-0442(2004)017<3169:sitmo>2.0.co;2

19448007, 2023, 2, Downloaded from https://agupubs.onlinelibrary.wiley.com/doi/10.1029/2022GL101773 by NHMRC National Cochrane Australia, Wiley Online Library on [29/01/2023]. See the Terms and Conditions (https://onlinelibrary.wiley.com/terms-and-conditions) on Wiley Online Library for rules of use; OA articles are governed by the applicable Creative Commons License